Early View publication on www.interscience.wiley.com
(issue and page numbers not yet assigned;
citable using Digital Object Identifier – **DOI**)

phys. stat. sol. (a), 1–8 (2008) / **DOI** 10.1002/pssa.200777855

physica status solidi a
www.pss-a.com
applications and materials science

Imaging ellipsometry: quantitative analysis

L. Asinovski[*,1], **D. Beaglehole**[2], **and M. T. Clarkson**[3]

[1] Semiconsoft, Inc. Southborough, MA 01772, USA
[2] Beaglehole Instruments, Wellington, New Zealand
[3] Industrial Research Ltd., Lower Hutt, New Zealand

Received 16 July 2007, revised 3 December 2007, accepted 17 December 2007
Published online ■■■

PACS 07.60.Fs

[*] Corresponding author: e-mail Leo.Asinovski@semiconsoft.com, Phone: +1 617 388 6832, Fax: +1 603 710 7717

Imaging ellipsometry (IE) combines spatial resolution of optical microscopy with thin-film measurement capabilities of ellipsometry. It has gained significant interest in recent years and is been used for a wide range of applications from biotechnology to semiconductor metrology. Traditionally, IE is used either as a qualitative technique – not unlike polarized microscopy or Surface Plasmon Resonance (SPR) – with "ellipsometry images" showing surface topology variation, or as a quasi-quantitative technique where the change in "ellipsometry images" is used to deduce the change in film thickness. In this paper we give a brief critical review of different measurement systems configurations from the point of view of their fitness to quantitative IE measurement. We discuss the methods of calibration and correction that enable to achieve a truly quantitative IE measurement. We show that a fast and reliable quantitative IE can be practically implemented. It is consistent and can be used in lieu of a classical single point ellipsometry in many applications.

1 Introduction Imaging ellipsometry (IE) combines high spatial resolution of optical microscopy with thin-film measurement capabilities of the ellipsometry. This combination is significantly important for a range of applications: a complete microarray can be quickly and reliably measured without using dyes that required for traditional fluorescent spectroscopy; optical properties uniformity and lubricant thickness in magnetic head applications can be reliably controlled; uniformity of thin-film thickness of complete wafer can be measured using much smaller test pads or, in some cases, directly on device areas [1–9]. In many cases, like measurement of the liquid-surface interface dynamics (e.g. surfactants) IE provides unique capability, in others – a much-improved speed of the measurement and/or quality of the results. High spatial resolution of IE adds a new dimension to ellipsometry measurement but this comes at a price – the measurement conditions are fundamentally non-ideal: angle of incidence (AOI) is changing across the image, high numerical aperture (NA) required to achieve spatial resolution mean that measurements are averaged over a cone of AOIs, oblique incidence distorts the image and causing depth of focus problems, optical components has non-uniformities and residual birefringence [10]. As a result IE has, in general, a sensitivity of a classical, single measurement point ellipsometry (SPE) but lacks its absolute accuracy, i.e. IE is primarily used as a qualitative technique for relative measurements.

Historically, new developments in ellipsometry technique or expansion in application area were bringing new challenges related to measurement conditions correction and calibrations: transition from a null to photometric automated measurement system required error propagation analysis [11]; transition from single wavelength (SWE) to spectroscopic (SE) ellipsometry brought an issue of retardation dispersion (especially in the case of multi-channel, parallel measurement) [12]; semiconductor metrology application of the SE required the measurement in small test areas (~40 × 40 μm^2) with high throughput that brought an issue of wavelength resolution and AOI averaging [13]. IE is a natural evolution of ellipsometry measurement technique, so it is not surprising that it is facing similar problems. Like SE that combined ellipsometry with spectroscopy, IE is a hybrid of ellipsometry and microscopy that brings new capabilities and challenges.

In this paper we give a brief critical review of different measurement system configurations from the point of view of their fitness to quantitative IE measurement. The methods of calibration and correction to achieve a truly quantitative IE measurement are discussed. We show that a fast and reliable quantitative IE can be implemented in practice; it is consistent and can be used in lieu of a "regular" single point ellipsometry in many critical applications. We show that an accurate data analysis of the full image (~2 million points) can be performed fast (typically in a few minutes) and accurately, without any approximations. Finally, we show experimental data of the fully quantitative IE.

2 Imaging ellipsometry systems: quantitative vs. qualitative measurements IE offers unique capabilities that extend classical ellipsometry but the measurements are more complex and require some modification of the approach and configurations commonly used in ellipsometry.

To quantify the change in polarization state one measures r_p/r_s value, where r_p, r_s are reflectances of light polarized in-plane of incidence and perpendicular (senkrecht) to the plane of incidence, respectively. The main equation of ellipsometry is expressed in the following form:

$$r = r_p/r_s = \mathrm{Re}\,(r) + \mathrm{Im}\,(r) = \tan\,\Psi\, e^{i\Delta}$$

$$\text{or} \quad X = \alpha\,\mathrm{Re}\,(r)\,; \qquad Y = \alpha\,\mathrm{Im}\,(r)\,; \tag{1}$$

where $\alpha = 1/(1 + |r|^2)$.

Δ, Ψ are frequently referred to as *ellipsometry angles* and **X,Y** as *ellipsometry parameters*. They are directly related using following equations:

$$X = \sin 2\Psi \cos\Delta\,; \qquad Y = \sin 2\Psi \sin\Delta\,.$$

Ψ, X are sensitive to polarization contrast, while Δ, Y are primarily sensitive to phase difference.

We will now review some of the measurement systems configurations to illustrate the difficulties and discuss the modifications needed to adopt these systems for IE measurement.

2.1 Null ellipsometry configuration has one very attractive characteristic that frequently makes it a system of choice for new complex measurements: it allows to sidestep the analysis/calibration of the system artefacts. This is made possible by taking measurements at several quadrants (two or four) and averaging the results – such procedure has been shown to cancel out misalignments and other internal system artefacts [11].

Null ellipsometry uses a static PCSA (Polarizer-Compensator-Sample-Analyzer) system with positions of analyzer and polarizers adjusted to achieve light extinction (null position).

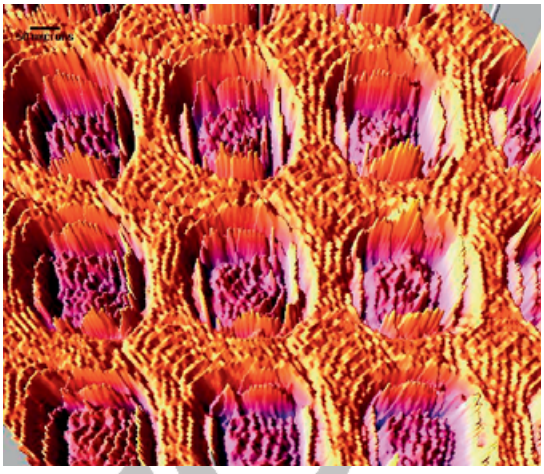

Figure 1 (online colour at: www.pss-a.com) Delta map taken with a laser (532 nm) null ellipsometer (~1.5 × 2 μm resolution). Sample is 4000 Å oxide on Si; a grid of 100 × 100 μm areas (~400 Å deep) is etched in SiO_2. The picture shows clear effects of diffraction (structure inside the etched areas) and speckles.

There are two problems with this configuration:

a) High intensity is required for accurate measurement- this means the use of a laser source. Imaging of the sample with a surface structures or regular pattern using coherent light creates speckles that introduce additional artefacts and reduce resolution. An example of high-resolution ellipsometry (Delta) image of a sample with regular pattern (Fig. 1) shows the effects of coherent light related diffraction.

b) In classical null ellipsometry, polarizer/analyzer azimuths need to be separately adjusted for each of the measurement points – hundreds of thousands in case of imaging ellipsometry; such approach would be impractical. This condition can be mitigated in the modern null ellipsometer system by taking off-null measurements at several points and finding the null position by using a fit to a parabolic function. For small deviations from the null position light intensity (I) can be expressed as $I \sim ((\delta A)^2 + (\delta P)^2 \sin^2(2A))$, where A is the angle of analyzer and δA, δP are the deviations of analyzer and polarizer angle, respectively, from the null position. With this approach, one can, fundamentally, take a limited number of intensity measurements at different positions of polarizer/analyzer and calculate a null position at all points of the image. In case of a non-uniform sample one needs to take a large number of measurement at different analyzer/polarizer positions in order to have enough information to calculate all null positions. For large deviations of polarizer/analyzer from the null position the dependence becoming more complex: $I \sim |r_p \cos A \cos P + r_s \sin A \sin P|^2$ and includes the properties of the sample.

The salient point is that, in practice, some measurements will be inaccurate for highly non-uniform surface structures.

2.2 Off-null PCSA imaging ellipsometer PCSA (Polarizer, retarder, sample and analyser) ellipsometer is using the same basic configuration as a null ellipsometry system. However, instead of finding the "null position" – intensity measurements at four fixed positions of the compensator allow to calculate X- and Y-values directly

$$X = (I_0 - I_{90})/(I_0 + I_{90}) ; \qquad Y = (I_{30} - I_{210})/(I_{30} + I_{210}) , \qquad (2)$$

where I_0, I_{90}, I_{30}, I_{210} are intensities measured at compensator angle of 0, 90, 30 and 210 deg, respectively [14, 15]. Although configuration and measurements are similar to null-ellipsometry – the approach is very different: no null position is calculated and only four measurements are required. The advantage is that X-, Y-values can be determined accurately in a wide range of variation (highly nonuniform sample) and high light intensity is not required – can use incoherent light source like LED. The drawback is the lack of zone averaging. Typically, the main contributing artefact is the stray birefringence of the elements. It is significant, since birefringence varies across the field of view. Fortunately, birefringence effect can be easily removed by differencing calibration images of the straight-through measurement or calibration sample. Off-Null PCSA system is as simple and robust as null-ellipsometry but the measurements are faster and the quality is improved. Compensator chromatism limits the spectral range of this system and some kinetics monitoring applications may require faster measurements. Several modulation measurement systems had been recently proposed, including the use of rotating analyzer and phase modulation. Rotating-analyzer system implementation [16] is similar to a classical ellipsometry but its application is somewhat limited due to difficulty of using rotating polarizer element for high-resolution imaging. Phase modulation seems a better fit but is has to be modified for use in imaging ellipsometry.

2.3 Coherent phase modulation imaging ellipsometer (CPM) allows fast and accurate measurements in the wide spectral range; it uses photoelastic modulator and synchronized (strobe) measurements [17, 18].

Imaging ellipsometers usually use CCD or CMOS detectors to take a sequence of appropriate 2D images from which the ellipsometry parameters can be obtained. The polarisation state is set by birefringence in a mechanically oscillating transparent longitudinal bar – photoelastic modulator (PEM). Maximum strain in the bar occurs at the bar-centre, which undergoes no centre-of mass displacement. Driving the bar with well regulated power can vary the amplitude of mechanical oscillation.

A typical PEM is made from fused silica and covers a wide wavelength range (180 to 2000 nm). The modulation frequency is typically 50 kHz using a 50 mm bar length. The oscillation frequency is too high to use with CCD frame capture with exposure times a fraction of the modulation time, but coherent flash illumination or gated detector can be synchronized with PEM modulation to strobe-measure images at specific times in modulation cycle. Intensity variation $I(t)$ in this system can be expressed by following equation:

$$I(t) = I_{dc} + X \sin(A \sin(\omega t)) + Y \cos(A \sin(\omega t)) , \qquad (3)$$

where A, ω are the amplitude and frequency, respectively, of photoelastic modulator; I_{dc} is unmodulated intensity. In this case Eq. (2) can be used again to determine X-, Y-values but intensity subscripts correspond to ωt positions rather than compensator azimuth angle.

Differencing images to remove backgrounds is again, like zone averaging, an important technique that allows removing of instrument artefacts.

3 Imaging ellipsometry: data analysis Imaging ellipsometry combines capabilities and faces challenges of classical ellipsometry and microscopy. Depending on measurement requirements it can be used as a qualitative technique, quasi-quantitative or a fully quantitative technique. In a latter case, it utilizes full capabilities of classical ellipsometry and microscopy but requires more accurate calibration, corrections and calculations.

3.1 Qualitative approach High sensitivity of ellipsometry, in particular Δ or Y parameters, to the thickness of thin layers, allows the use of their images to qualitatively review the samples (typically patterned or nonuniform structures).

Using "ellipsometry images" is similar to BAM or SPR but does not require near-Brewster angle measurements. At the same time ellipsometry offers ~10 times higher sensitivity than BAM. Different configuration has been proposed to further improve sensitivity [19–23], e.g. TIRE (Total Internal Reflection Ellipsometry) achieve ~30 times increase of sensitivity (this is ~300 times higher than BAM) that is comparable or exceeding SPR performance (Fig. 2).

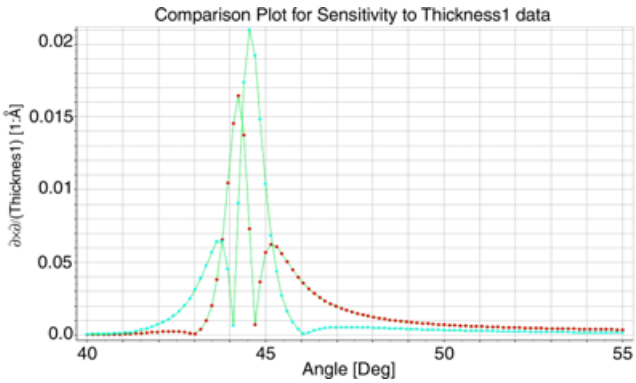

Figure 2 (online colour at: www.pss-a.com) Sensitivity of X (red circles), Y (blue squares) ellipsometry parameters to thickness of layer (water) formed in SPR configuration. Glass prism, 480 Å Au layer. TIRE configuration measurement shows ~30 times increase in sensitivity vs. standard ellipsometry measurement and >300 times better than BAM sensitivity.

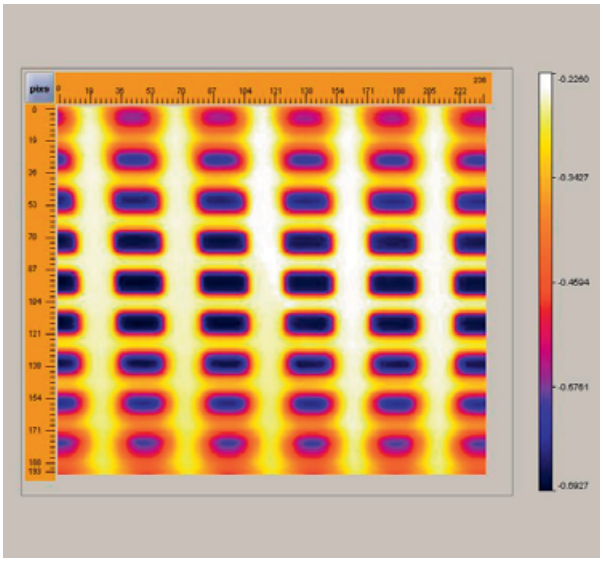

Figure 3 (online colour at: www.pss-a.com) Raw Y image taken at 62.5 deg (wavelength 625 nm) of the etched Sio2 film. Etched areas are 100 × 100 µm squares (distortion is caused by the oblique angle of incidence). Image resolution is 7 µm/pixel. Top and bottom of the image is defocused showing the limits of the DOF.

Using qualitative approach does not require corrections, calibrations and inferring of thickness data from the measurements. Still, one has to correct the raw images for distortion and depth of focus. Angular distortion is easy to correct by rescaling the images; as a result, resolution in the direction perpendicular to plane of incidence is reduced to resolution in the plane of incidence (if high resolution is critical – linescan in the direction perpendicular to the plane of incidence allows to capture the data).

Depth of the focus (DOF) is more difficult to correct and requires taking a series of images by either moving the sample or adjusting focal length of objective, and processing/stitching these images using a special algorithm [24]. Uncorrected Y image on Fig. 3 shows the effect of the depth of the focus and angular distortion.

It is instructive to review the dependence of lateral resolution (L) and DOF on numerical aperture NA (A): $L = c\lambda/A$; DOF = $\lambda/(A^2 \sin\theta)$ where $c = 1.2–1.6$ (higher coefficient for coherent illumination), λ – light wavelength, θ – angle of incidence [25]. The results are presented in Table 1. High resolution requires large (~0.35) NA that may have significant effect on values of ellipsometry parameters unless AOI is low.

Table 1 Dependence between resolution, NA and depth of focus (circular aperture and incoherent light) for 530 nm, 55° angle of incidence.

cone angle (deg)	resolution (µm)	DOF* (µm)
10	7	80
20	3.5	20
40	1.7	5.5

* depth of focus (area of sample in focus)

Qualitative approach may be useful in some cases that require review of the patterned structured or detection of the features on the surface but it does not provide any values of the physical parameters e.g. thickness or optical properties. In the limited number of practically important cases qualitative approach can be easily extended to a quasi-quantitative one.

3.2 Quasi-quantitative approach Quasi-quantitative approach exploits the fact that there is a linear relation between small change of layer thickness (δT) and change in $\Delta(\delta\Delta)$: $\delta\Delta = k\,\delta T$, where k is a constant that depends on optical properties of the layer's material. This dependence is illustrated on Fig. 4. Once the k value for specific material is determined e.g. using calibration samples, one can use relative/differential measurement of Delta or Y and easily calculate thickness difference. The approach is working well for thin oxides or protein growth but has limited applicability for static measurements. The obvious advantage is fast calculation, no need for accurate X (Psi) measurement and automatic correction (differential measurement) of instrument artefacts.

This method can also be extended to static measurement of nonuniform layer of known material. In this case, again, the change in Delta (Y) can be easily and quickly translated in thickness variation. However, hardware artefacts are not corrected (not a differential measurement) – the only advantage is a quick calculation.

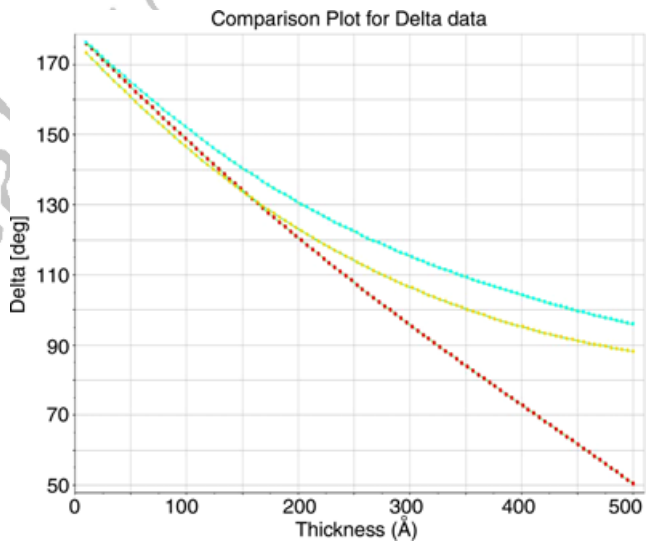

Figure 4 (online colour at: www.pss-a.com) Relation between Delta and thickness (d) of a thin film. CdS (red squares) and oxide (green dots) at 632 nm, oxide (yellow dots) at 425 nm. The thickness range is 0–500 Å (x-axis), Delta (Y-axis). Delta = $f(d)$ is generally nonlinear for dielectric material and depends on refractive index value. At the same time, the dependence is smooth (within the cycle) and linear dependence between small thickness and Delta changes can be used.

Quasi-quantitative approach is a powerful tool for analyzes of many applications but it has significant limitations. To unlock full power of ellipsometry technique one needs to use a full quantitative approach.

3.3 Quantitative approach treats imaging ellipsometry as a *bona fide* ellipsometry technique, in a classical sense, which has additional benefit of high-resolution imaging. This, of course, requires factoring in or correction of non-ideal measurement conditions and attention to calculations optimization.

Image correction approach to DOF extension and angular distortion are, essentially, the same as in qualitative analysis case. The only difference is that angular distortion correction is better applied to calculated results (e.g. thickness) map – not original measured data. Distortion correction includes image rescaling i.e. interpolation and averaging. Since dependence between measured data (M) and calculated parameters (P) is nonlinear (with few exception e.g. very thin films) it is better to apply correction to results.

Classical ellipsometry typically assume ideal measurement conditions, i.e. accurately known value of AOI and quasi-collimated incident beam. Any deviations from ideal measurement conditions are minimized. For example, in semiconductor metrology the measurement in small 40×40 μm test areas requires a focused beam with high NA but the receiving arm can use aperture to limit the effective NA (at the expense of intensity) or multi-AOI approach is used. As a result, a near ideal measurement conditions are achieved. Imaging ellipsometry requires high aperture for high resolution (see Table 1). To reduce the effect of the AOI averaging, one can use the same approach as described in the example above – only using collimated bean in illuminating arm. However, this may be possible only for single wavelength systems because of the light intensity. In standard ellipsometry, one can average all the

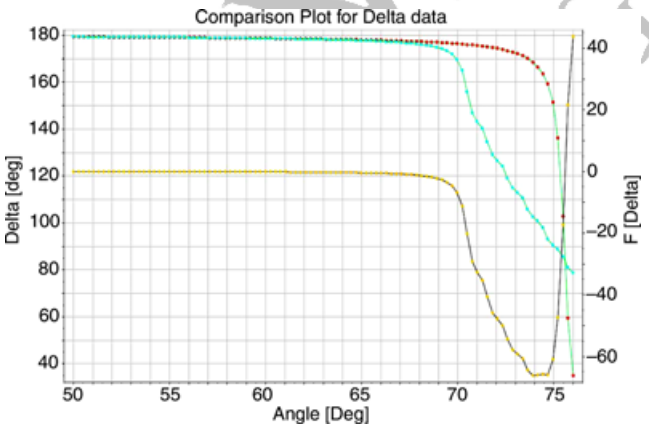

Figure 5 (online colour at: www.pss-a.com) Effect of the cone AOI averaging on Delta simulation. Cone angle is 10 deg (NA = 0.1). Yellow line shows the difference between "ideal" and "averaged" results for Delta (the effect is pronounced for AOI > 70°).

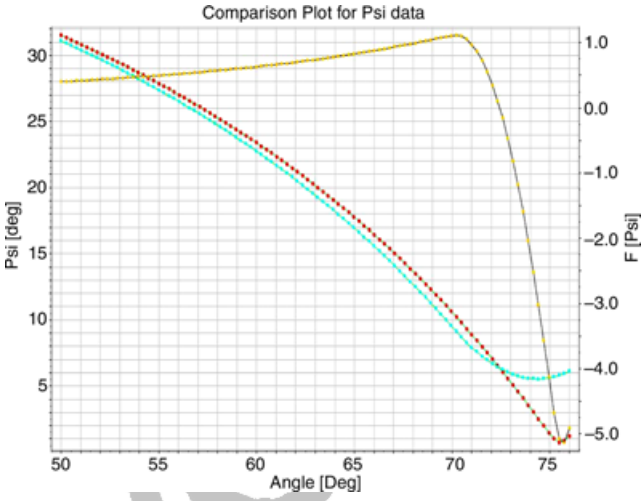

Figure 6 (online colour at: www.pss-a.com) Effect of the cone AOI averaging on Psi simulation. Cone angle is 10 deg (NA = 0.1). Yellow line shows the difference between "ideal" (red squares) and "averaged" (blue dots) results.

intensity from the measured area, while in case of the IE one measures 10^6 points instead and, therefore, intensity has to be several orders of magnitude higher. In practice, all spectroscopic or multi-wavelength IE have to use angle averaging and one needs to take angle averaging into account during calculation procedure. The effect of AOI averaging on Delta and Psi (Figs. 5, 6) shows that it is relatively small, but not negligible, for AOI below Brewster angle. In fact, most high-resolution measurements (including those for qualitative analysis) are taken at AOI ~50 deg to avoid the overlapping of Brewster angle and conform to physical limitation of the optical system configuration.

The implementation of AOI averaging depends on the measurement system – since actually averaged values are the measured intensities (not X, Y or Delta, Psi values directly). In case of X, Y parameters one can use Eq. (2) to see that direct X, Y is possible as well since

$$I_0 + I_{90} \approx I_{30} + I_{210} = \text{const}$$

$$(\langle I_0\rangle - \langle I_{90}\rangle)/(\langle I_0\rangle + \langle I_{90}\rangle) \approx \langle I_0 - I_{90}\rangle/\text{const} = \langle X\rangle$$

$$(\langle I_{30}\rangle - \langle I_{210}\rangle)/(\langle I_{30}\rangle + \langle I_{210}\rangle) \approx \langle I_{30} - I_{210}\rangle/\text{const} = \langle Y\rangle$$

where $\langle\,\rangle$ indicates averaging over AOIs.

This gives a very simple way of accounting for AOI averaging – one just need to calculate X-, Y-values for several angles within the range and take an average. However, this "brute force" approach increases the number of calculations dramatically (since calculations are repeated for every point).

Effect of the AOI averaging on X-, Y-values for thin SiO_2 layer is presented on Fig. 7. One can see that the effect of AOI averaging is somewhat similar to the increase of AOI. Indeed, the direct calculation shows that for low incidence angles, AOI averaging can be compensated by

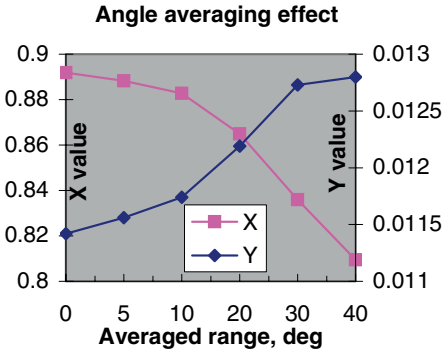

Figure 7 (online colour at: www.pss-a.com) Effect of angle averaging on *X*, *Y* parameters. Sample is 10 Å SiO_2/Si. Nominal AOI = 50°, wavelength 625 nm. Averaging range (*x*-axis) is a cone angle of incident light i.e. 20 deg means ±10° from nominal angle: range of [40–60] deg.

calculation of effective AOI. Results of the simulation for two oxide samples (10 Å and 1000 Å) presented in Table 2 shows that AOI averaging compensation using effective AOI approach is working well for small cone angles e.g. 10° that corresponds to ~7 μm resolution. For higher resolution – large cone angles – the measurement errors increases and direct averaging calculation maybe necessary to achieve high accuracy.

Another non-ideal measurement condition inherent to imaging ellipsometry is the change of the AOI along the sample. We are concerned here only with the change of the AOI in the plane of incidence, since any changes in the plane perpendicular to the plane of incidence (that can occur due to sample tilt) has very small or no effect on the measured parameters. AOI variation in the plane of incidence is fixed for the selected configuration of the optical system and magnification of the objective. There are several ways to correct this variation: one is to use a calibration sample and apply calibration results for correction of the AOI; another is to calculate AOI, as an additional calculated parameters, at each point.

Calibration approach is convenient in cases when the measured sample is complex and calculation of an additional parameter is not desirable (it can also slow down calculations). For calibration, one can use a thin-oxide

Table 2 AOI averaging compensation.

AOI cone angle, deg	effective AOI offset (°) sample 10 Å (1000 Å)	thickness error, Å sample 10 Å (1000 Å)
5	+0.34 (+0.44)	0 (+1)
10	+0.84 (+1.22)	–0.2 (+4)
20	+2.35 (+3.57)	–0.5 (+15)
30	+4.45 (+6.44)	–1.1 (+30)
40	+6.10 (+9.3)	–1.8 (+48)

Simulation is performed for 10 Å and 1000 Å SiO_2/Si samples, AOI = 50°, Wavelength = 625 nm. The oxide thickness and AOI are calculated to get the best fit to data with averaged AOI.

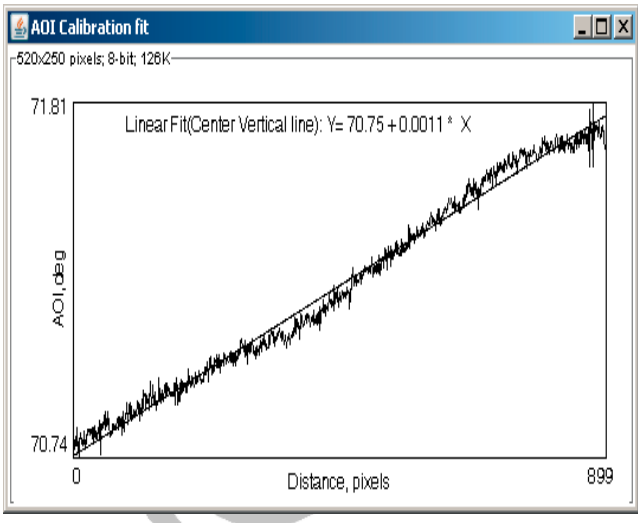

Figure 8 (online colour at: www.pss-a.com) AOI variation along the sample (native oxide on Si). The thickness of the oxide and AOI were calculated to extract AOI variation. Linear regression of the raw calculation results is used for AOI calibration.

sample, take the measurement at desired angle and magnification and calculate the thickness and AOI at each point. The results of such calibration are presented on Fig. 8 that shows a line scan of calculated AOI vs. pixels in the plane of incidence. Note, that the AOI averaging strategy during calibration should be the same as the one used during measurements. It is possible, for example, to use effective AOI to offset the effect of AOI averaging in calibration but one, in this case, is bound to effective AOI during the measurements as well. Linear dependence of AOI vs. pixels can be saved and used during the measurements to correct AOI of particular pixel. This approach effectively removes the AOI variation problem.

Direct calculation of the AOI along with other sample parameters is useful for ad-hoc measurements. However, it may lead to some flyers in the data.

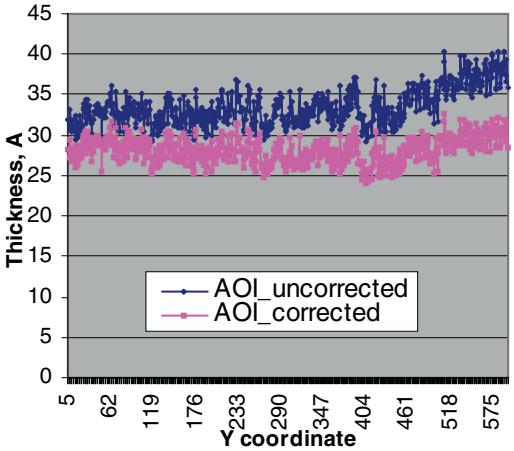

Figure 9 (online colour at: www.pss-a.com) Comparison of uncorrected and AOI corrected measurement of native oxide (ad-hoc AOI correction is used).

Table 3 Calculation results using quasi-quantitative and quantitative calculations. AOI = 70°, wavelength 625 nm, AOI cone angle 10° (resolution 7 μm), sample-native oxide on Si.

method	thickness (mean), *A*	thickness (s.d.), *A*
quasi-quantitative (use *Y* only)	34.5	4.2
quantitative	28.4	1.1

Calibration approach is preferable since it allows careful measurement of the AOI dependence on the known sample and appropriate averaging/smoothing of the data while ad-hoc direct AOI calculation maybe sensitive to measurement noise. However, in some cases, calibration data is not available and direct AOI calculation is the only viable option. An example of ad-hoc AOI calibration showing its effect on oxide thickness measurement is presented on Fig. 9.

Now with the AOI averaging corrected and AOI variation across the sample calibrated we should be able to have accurate quantitative analysis of ellipsometry data. It is instructive to review the measurement of a simple native oxide sample. Both qualitative and quasi-quantitative approaches can be used in this case. It is well known that while Delta sensitivity to thickness is high and sensitivity to AOI low, the Psi sensitivity is opposite. This is the rationale for using only Delta (or *Y*) data in quasi-quantitative method and ignoring Psi (*X*) with its sensitivity to AOI. With quantitative approach one can do all the corrections but it does not seem to gain much improvement since Delta that contains most information does not have sensitivity to AOI. However, there are two factors that we need to consider: a) Delta sensitivity to thickness is highest near Brewster angle but sensitivity to AOI is high at these angles too. Perhaps, we can utilize high sensitivity and correct the AOI. b) Psi (*X*) measurement can provide additional constraint to minimize the effect of measurement noise, etc. The results of the calculations on native oxide sample are presented in Table 3. The same measured data was processed using quasi-quantitative and full quantitative approach (calibrated AOI variation was used). The use of the quantitative approach results in more uniform oxide thickness (lower s.d.) values.

To verify the absolute accuracy of the imaging ellipsometry measurement we compared it with the results obtained with classical high-precision laser ellipsometer. For this experiment, we have used a 150 nm oxide sample: the oxide was thermally grown on the surface of a 25 × 25 mm silicon wafer (111 orientation) at 900 °C in a stream of oxygen. The measurements were carried out in air on a customised imaging ellipsometer manufactured by Beaglehole Instruments Ltd. The angle of incidence was 70° and wavelength of light 625 nm. The ellipsometer has an iris in the detection arm to adjust the depth of focus. This was set to about halfway of its adjustable range. Magnification was set to 1.0, corresponding to 148 pixels per 1 mm (along the direction perpendicular to the plane of incidence) – 7.75 μm/pixel. AOI variation calibration was performed using a 25 × 25 mm Si with native oxide prior to the sample measurement the same exact configuration of the measurement system. Single point measurements were taken using high-precision laser (632.8 nm) picometer system manufactured by Beaglehole Instruments. The picometer is using photoelastic modulation with lock-in amplifier detection system [26] and was calibrated using NIST traceable samples. The measurements were taken in five points (centre and 5 mm from centre in four directions) with the beam size ~1 mm. Imaging data was properly averaged (over 1 mm measurement sites) for comparison. The results are presented in Table 4 and show excellent agreement between the measurements.

Table 4 Calculation results using quasi-quantitative and quantitative calculations. AOI = 70°, wavelength 625 nm, AOI cone angle 10º (resolution 7 μm), sample – native oxide on Si.

measurement point (*x*,*y*) mm	imaging ellipsometry (thickness, Å)	reference ellipsometer (thickness, Å)
0, 0	1485	1487
–5, 0	1515	1517
0, –5	1497	1499
5, 0	1459	1461
0, 5	1470	1469

Quantitative analysis of imaging ellipsometry data is very calculation intensive; a special attention to optimiza-

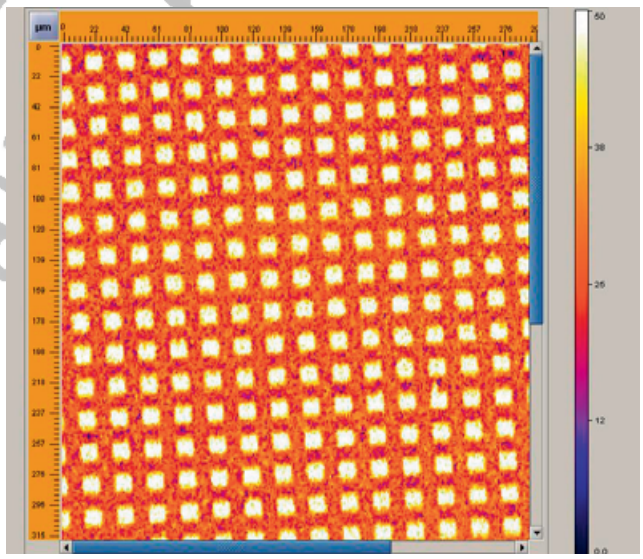

Figure 10 (online colour at: www.pss-a.com) Thickness map (Å) of the patterned thin organic silane films on silicon wafers. APTES (Aminopropyltrietoxysilane) was deposited via minopropyltriethoxysilane on a photolithographically patterned silica surface squares with APTES are ~10 μm with a 15 μm pitch. Delta/Psi measurements were taken at AOI = 56º and wavelength of 531 nm using Nanofilm's EP3 Imaging ellipsometer system. APTES thickness ~2 nm (monolayer is ~1 nm), there is a native oxide between APTES squares. Courtesy of Dr. Magnus Bergquist, Cornell University.

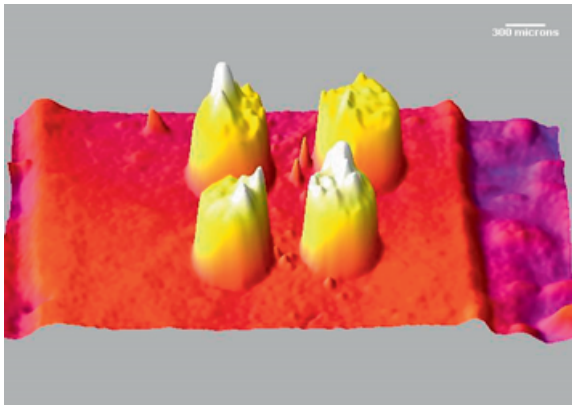

Figure 11 (online colour at: www.pss-a.com) Thickness topography of protein (streptavidin) binding spots. Measurement is taken with a Beaglehole Instruments Imaging ellipsometer using AOI = 70° and wavelength of 625 nm. AOI calibration is used in calculation. 4 nm protein/2 nm aminosilane/2 nm oxide/Si.

tion is required, given a very large data set (full image contain ~2 mil. pixels: 1200 × 1600 pixels to be precise) that need to be processed. Data analysis and image processing algorithms were implemented in TFCompanion software [26]. We found that Sun Microsystems' java HotSpot technology is perfectly suited for repetitive type of the calculations: after calculation of a few first points – the speed of the rest of calculation is dramatically increased. The calculation speed depends, of course, on filmstack, number of calculated parameters and hardware used. In calculations for this paper we used AMD 2800 CPU and 2GB RAM with Windows2000, all calculations were in 10 min range (typical speed is ~100 K pts/min).

Finally, quantitative approach has been used for analysis of several experimental data sets.

Patterned thin organic silane film on silicon wafers was measured at 56° at 531 nm. Delta, Psi data maps were used to calculate the thickness and AOI (ad-hoc correction) at all points. The results are presented on Fig. 10.

An example of a protein binding measurement is presented on Fig. 11. In this experiment the substrate (a 25 × 25 mm silicon wafer (100 orientation) with native oxide) was coated with an amino-silane (thickness of coating ~2 nm). Four spots of a functionalised vitamin were applied to the surface. After incubation the liquid spots were rinsed off the surface. The surface was then placed in a liquid-filled cell into which a solution of bovine serum albumen (BSA) was injected to bind to any remaining reactive sites on the surface. A protein (streptavidin) was then injected and binding to the spots was monitored. The surface was then rinsed, dried in nitrogen and stored in a dessicator. The X, Y measured maps were used to calculate the thickness of the protein layer, a previously measured AOI calibration was used to correct for AOI variation across the sample.

4 Conclusion Imaging ellipsometry extends capabilities of classical ellipsometry by combining it with optical microscopy. However, it is currently used primarily as a qualitative or quasi-quantitative technique. As a result, applications areas are limited and full potential of ellipsometry technique is not realized. In this paper we critically reviewed different measurement systems, discussed qualitative, quasi-quantitative and fully quantitative use of the IE. We have shown that fundamentally non-ideal IE measurement conditions can be corrected and accurate quantitative analysis consistent with a classical ellipsometry can be performed.

References

[1] D. van Noort, J. Rumberg, E. W. H. Jager, and C.-F. Mandenius, Meas. Sci. Technol. **11**, 801–808 (2000).
[2] Q. Zhan and J. R. Leger, Appl. Opt. **41**, 4443–4450 (2002).
[3] D. Schmaljohann, M. Nitschke, R. Schulze, A. Eing, C. Werner, and K.-J. Eichhorn, Langmuir **21**, 2317–2322 (2005).
[4] P. Karageorgiev, H. Orendi, B. Stiller, and L. Brehmer, Appl. Phys. Lett. **79**, 1730–1732 (2001).
[5] G. Jin, R. Jansson, and H. Arwin, Rev. Sci. Instrum. **67**, 2930–2936 (1996).
[6] M. C. Howland, A. W. Szmodis, B. Sanii, and A. N. Parikh, Biophysics J. **92**, 1306–1317 (2007).
[7] A. J. Choi, T. H. Ghong, Y. D. Kim, J. H. Oh, and J. Jang, J. Appl. Phys. **100**, 113529 (2006).
[8] K. Hinrichs, M. Gensch, N. Esser, U. Schade, J. Rappich, S. Kröning, M. Portwich, and R. Volkmer, Anal. Bioanal. Chem. **387**, 1823–1829 (2007).
[9] A. Albersdörfer, G. Elender, G. Mathe, K. R. Neumaier, P. Paduschek, and E. Sackmann. Appl. Phys. Lett. **72**, 2930–2932 (1998).
[10] M. Harke, R. Teppner, O. Schulz, H. Motschmann, and H. Orendi, Rev. Sci. Instrum. **68**, 3130–3134 (1997).
[11] R. M. A. Azzam and N. M. Bashara, Ellipsometry and Polarized Light (North-Holland Publ. Co., Amsterdam, 1979).
[12] R. W. Collins, Thin Solid Films **313/314**, 18–32 (1998).
[13] T. Piwonka-Corle (KLA-Tencor), US Patent 5,910,842 (1999).
[14] D. Beaglehole, Rev. Sci. Instrum. **59**, 2557–2559 (1988).
[15] C. Chou, H.-K. Teng, C.-J. Yu, and H.-S. Huang, Opt. Commun. **273**, 74–83 (2007).
[16] W. Chegal, Y. J. Cho, S. B. Oh, H. M. Cho, Y. W. Lee, and S. H. Kim, Meas. Sci. Technol. **16**, 716–722 (2005).
[17] D. Beaglehole, US Patent Application #20050134849 (2004).
[18] C.-Y. Han and Y.-F. Chao, Rev. Sci. Instrum. **77**, 023107 (2006).
[19] A. V. Nabok, A. Tsargorodskaya, A. K. Hassan, and N. F. Starodub, Appl. Surf. Sci. **246**, 381–386 (2005).
[20] H. Arwin, Appl. Opt. **43**, 3028–3036 (2004).
[21] L. Kempen, US patent #6,594,011 (2000).
[22] S. Otsuki, Appl. Opt. **44**, 1410–1415 (2005).
[23] S. Venkatasubbarao, J. Biomed. Opt. **11**, 014028 (2006).
[24] B. Forster, D. Van Ville, J. Berent, D. Sage, and M. Unser, Microsc. Res. Tech. **65**, 33–42 (2004).
[25] M. Born and E. Wolf, Principles of Optics (Cambridge Univ. Press, 2002).
[26] Information on TFCompanion software and ellipsometer systems http://www.semiconsoft.com.